 CMES, vol.102, no.4, pp.291-330, 2014

Fatigue Crack Growth Reliability Analysis by Stochastic Boundary Element Method

Xiyong Huang[1], M. H. Aliabadi[2] and Z. Sharif Khodaei[3]

Abstract: In this paper, a stochastic dual boundary element formulation is presented for probabilistic analysis of fatigue crack growth. The method involves a direct differentiation approach for calculating boundary and fracture response derivatives with respect to random parameters. Total derivatives method is used to obtain the derivatives of fatigue parameters with respect to random parameters. First-Order Reliability Method (FORM) is applied to evaluate the most probable point (MPP). Opening mode fatigue crack growth problems are used as benchmarks to demonstrate the performance of the proposed method.

Keywords: Dual boundary element method, Fatigue crack growth, Reliability.

1 Introduction

Probabilistic Fracture Mechanics (PFM) is a recognised tool for realistic evaluation of fracture response and reliability of cracked structures Feng, Garbatov, and Guedes Soares (2012); Dong and AtIuri (2013); Leonel, Chateauneuf, and Venturini (2012); Guo and Chen (2013); Paffrath and Wever (2012); Hombal, Wolfe, Ling, and Mahadevan (2012); Li, Xiang, Wang, Zhang, and Liu (2013); Graham-Brady and Liu (2013); Katsuyama, Itoh, Li, Osakabe, Onizawa, and Yoshimura (2014). Using PFM, statistical uncertainties can be incorporated in engineering design and evaluation. The theory of fracture mechanics provides a relationship between the maximum load acting on a structural component and the size and location of a crack in that component, while the probability theory evaluate the randomness in crack size, loads and material properties affect the integrity of cracked structures. In PFM, the derivatives of stress intensity factor (SIF) or J-integral are

[1] Department of Aeronautics, Imperial College London, South Kensington, London SW7 2AZ, U.K.
[2] Department of Aeronautics, Imperial College London, South Kensington, London SW7 2AZ, U.K. E-mail: m.h.aliabadi@imperial.ac.uk
[3] Department of Aeronautics, Imperial College London, South Kensington, London SW7 2AZ, U.K. E-mail: z.sharif-khodaei@imperial.ac.uk

often required for probabilistic analysis Besterfield, Liu, Lawrence, and Belytschko (1990); Chen, Rahman, and Park (2001); Grigoriu, Saif, El Borgi, and Ingraffea (1990); Provan (1987). These two fracture parameter are required for obtaining the gradient of performance function with respect to random parameters in first- and second order reliability methods (FORM/SORM).

As for fatigue reliability analysis, different types of uncertainty such as physical variability (material properties, loading), data uncertainty (crack detection uncertainty, sparse data), and model uncertainty (SIF, crack growth law) errors are all contributing to that aspect. Bayesian network has been used in two different ways in PFM: 1) probabilistic crack growth prediction (forward problem) Rebba and Mahadevan (2008) and 2) quantifying the uncertainty of the model parameters, i.e. model calibration (inverse problem) Sankararaman, Ling, Shantz, and Mahadevan (2011). Sankararaman, Ling, and Mahadevan (2011) used the calibrated model for probabilistic crack growth prediction (combining both inverse and forward problems) using a dynamic Bayesian network including all three types of uncertainty. Several different crack growth models were efficiently used with Bayes network: finite element anlysis, surrogate model analysis and crack growth law. Probabilistic damage prediction can then be used in effective prognosis under uncertainty to predict the remaining useful like of the structure.

Most previous research has focused on advanced probabilistic algorithms coupled with finite element method because of its generality and popularity. A probabilistic finite element method coupled with FORM has been developed by Besterfield, Liu, Lawrence, and Belytschko (1991); Harkness, Belytschko, and Liu (1992) for the reliability analysis of the fatigue crack growth. The finite element analysis and the reliability calculation is linked through a response surface program using Hermite polynomials for the fatigue reliability of marine structures by Schall, Rackwitz, Scharrer, and Ostergaard (1991). Zhu, Lin, and Lei (1992) assumed the material resistance to fatigue crack growth and the time-history of the stress are random to obtained the analytical expressions for a randomized Paris-Erdogan law. Peng, Geng, Liyan, Liu, and Lam (1998) combined the stochastic finite element method with a second-order three-moment reliability analytical model to investigate the fatigue strength reliability of a gear teeth subjected to bending. More recent advances have been reported in Lua, Liu, and Belytschko (1993) which combines the mixed boundary integral equations with the first-order reliability method for probabilistic crack growth analysis and the least-squares fitting routine is used to obtain the first-order response-surface model of the random parameters.

In contrast, boundary element method has emerged as the most efficient technique for the evaluation of stress intensity factor and crack growth analysis in the context of linear elastic fracture mechanics Benedetti, Aliabadi, and Davi (2008);

Dirgantara and Aliabadi (2000); Fedelinski, Aliabadi, and Rooke (1996); Sfantos and Aliabadi (2007); Wen, Aliabadi, and Rooke (1998a,b). Portela and Aliabadi Portela, Aliabadi, and Rooke (1992, 1993) and Mi and Aliabadi (1994) presented an application of the Dual Boundary Element Method (DBEM) to the analysis of mixed-mode crack growth in 2D and 3D linear elastic fracture mechanics, where the crack growth processes were simulated with an incremental crack extension analysis based on the maximum principal stress criterion for 2D and minimum strain energy density criterion for 3D.

In this study, a dual boundary element method combined with FORM to predict probability of fatigue failure for mode-I crack growth is presented. The response gradient of performance function is determined by the total derivative method (TDM). The derivative of fracture parameters with respect to crack size, required for probabilistic analysis, is calculated using the implicit differentiation method (IDM). The randomness in the initial crack length, final crack length, fatigue crack growth parameters and the applied stress are considered in the present work. Other random parameter of the problem can be included. The Hasofer–Lind–Rackwitz–Fiessler algorithm is used to find the most probable point, referred to as the reliability index. The efficiency and accuracy of the proposed method on a classical mode I fatigue problem is demonstrated by comparison with Monte Carlo simulation (MCS) .

2 The dual boundary element method

2.1 Boundary element formulation

The basic Boundary Integral Equations can be written as Aliabadi (2002):

$$C_{ij}(\mathbf{x}')u_j(\mathbf{x}') + \int\!\!\!\!\!\!-_{\Gamma} T_{ij}(\mathbf{x}',\mathbf{x})u_j(\mathbf{x})d\Gamma(\mathbf{x}) = \int_{\Gamma} U_{ij}(\mathbf{x}',\mathbf{x})t_j(\mathbf{x})d\Gamma(\mathbf{x}) \tag{1}$$

where $\int\!\!\!\!\!\!-_{\Gamma}$ stands for Cauchy principle value integral, $C_{ij}(\mathbf{x}')$ is a tensor, dependent on the boundary shape at the source point $\mathbf{x}'$, u_j and t_j are components of displacements and tractions, respectively; $T_{ij}(\mathbf{x}',\mathbf{x})$ and $U_{ij}(\mathbf{x}',\mathbf{x})$ are the fundamental solutions for elastostatics.

The Dual Boundary Element Method (DBEM) has been developed to overcome the problems created by the analysis of crack domains without the need to use sub-regions. The usual displacement equation is now replaced with the traction equation on one of the crack surfaces.

$$\frac{1}{2}u_i(\mathbf{x}') + \frac{1}{2}u_i(\mathbf{x}'') + \int\!\!\!\!\!\!-_{\Gamma} T_{ij}(\mathbf{x}',\mathbf{x})u_j(\mathbf{x})\,d\Gamma(\mathbf{x}) = \int_{\Gamma} U_{ij}(\mathbf{x}',\mathbf{x})t_j(\mathbf{x})\,d\Gamma(\mathbf{x}) \tag{2}$$

$$\frac{1}{2}\sigma_{ij}\left(\mathbf{x}'\right)+\frac{1}{2}\sigma_{ij}\left(\mathbf{x}''\right)+\oint\!\!\!\!\!\!=_{\Gamma} S_{kij}(\mathbf{x}',\mathbf{x})u_k\left(\mathbf{x}\right)d\Gamma\left(\mathbf{x}\right)$$
$$=\oint\!\!\!\!\!\!= D_{kij}(\mathbf{x}',\mathbf{x})t_k\left(\mathbf{x}\right)d\Gamma\left(\mathbf{x}\right) \tag{3}$$

where $\oint\!\!\!\!\!\!=_{\Gamma}$ stands for Hadamard principle value integral.

The dual integral equations (2) and (3) will be evaluated for a source point $\mathbf{x}'$ on a smooth crack boundary to give the DBEM equations; where D_{kij} and S_{kij} are formed from the derivatives of the fundamental solutions $U_{ij,k}$ and $T_{ij,k}$. The detail of fundamental solutions T_{ij}, U_{ij}, D_{kij}, S_{kij} and Jacobian of Transformation J are shown in Appendix A:.

In BEM, a transformation of the system equations leads to an integral equation, evaluated only on the boundary of the domain Γ. In order to use the BEM, only the boundary of the body needs to be discretised into elements. Equation 1 can be discretised using quadratic boundary elements characterised by shape functions $M^n(\xi)$ and Jacobian $J^\gamma(\xi)$, with ξ the local dimensionless variable, leading to the following boundary integral equations:

$$C_{ij}(\mathbf{x}')u_j(\mathbf{x}')+\sum_{\gamma=1}^{M}\sum_{n=1}^{3}u_j^{\gamma n}(\mathbf{x})\mathrm{P}_{ij}^{\gamma n}=\sum_{\gamma=1}^{M}\sum_{n=1}^{3}t_j^{\gamma n}(\mathbf{x})\mathrm{Q}_{ij}^{\gamma n}\qquad i,j=1,2 \tag{4}$$

where the coefficient $\mathrm{P}_{ij}^{\gamma n}$ and $\mathrm{Q}_{ij}^{\gamma n}$ are defined in terms of integrals over Γ, where $d\Gamma(\mathbf{x})$ becomes $J^\gamma(\xi)d\xi$; that is

$$\mathrm{P}_{ij}^{\gamma n}=\int_{-1}^{+1}T_{ij}(\mathbf{x}',\mathbf{x}(\xi))M^n(\xi)J^\gamma(\xi)d\xi$$
$$\mathrm{Q}_{ij}^{\gamma n}=\int_{-1}^{+1}U_{ij}(\mathbf{x}',\mathbf{x}(\xi))M^n(\xi)J^\gamma(\xi)d\xi \tag{5}$$

Equations (2) and (3) can also be discretised using quadratic boundary elements characterised by $M^n(\xi)$ and $J^\gamma(\xi)$, leading to the following boundary integral equations:

$$\frac{1}{2}u_i(x')+\frac{1}{2}u_i(\mathbf{x}'')+\sum_{\gamma=1}^{M}\sum_{n=1}^{3}u_j^{\gamma n}(\mathbf{x})\mathrm{P}_{ij}^{\gamma n}=\sum_{\gamma=1}^{M}\sum_{n=1}^{3}t_j^{\gamma n}(\mathbf{x})\mathrm{Q}_{ij}^{\gamma n}\qquad i,j=1,2 \tag{6}$$

$$\frac{1}{2}t_i(x')+\frac{1}{2}t_i(\mathbf{x}'')+\sum_{\gamma=1}^{M}\sum_{n=1}^{3}u_k^{\gamma n}(\mathbf{x})\mathrm{V}_{kij}^{\gamma n}=\sum_{\gamma=1}^{M}\sum_{n=1}^{3}t_k^{\gamma n}(\mathbf{x})\mathrm{W}_{kij}^{\gamma n}\qquad k,i,j=1,2 \tag{7}$$

where the coefficient $\mathrm{V}_{kij}^{\gamma n}$ and $\mathrm{W}_{kij}^{\gamma n}$ are defined as:

$$\mathrm{V}_{kij}^{\gamma n} = \int_{-1}^{+1} S_{kij}(\mathbf{x}', \mathbf{x}(\xi)) M^n(\xi) J^\gamma(\xi) d\xi$$
$$\mathrm{W}_{kij}^{\gamma n} = \int_{-1}^{+1} D_{kij}(\mathbf{x}', \mathbf{x}(\xi)) M^n(\xi) J^\gamma(\xi) d\xi \tag{8}$$

Each of the boundary element equations contain either unknown displacement or traction value. However, from boundary condition given for each system, one of the values at each node can be found, giving a linear system of equations which may be solved using a standard method. The system can be written in matrix form as

$$\mathbf{A}\ \ \mathbf{X} = \mathbf{F} \tag{9}$$

In this equation, the vector $\mathbf{F}$ is evaluated from the application of the known boundary conditions to the system of equation, $\mathbf{X}$ is the vector of unknown values and $\mathbf{A}$ is the coefficient matrix. Although any standard linear algebraic routine can be used to solve the above system, the *LU* decomposition method is used here since the repeated computations with only forward and backward substitution is required for each of the derivatives analysis.

2.2 Derivatives of dual boundary integral equations

The response derivatives with respect to a set of random parameters Z_m, $(m = 1....N_v)$, where N_v is the number of random parameters, will be computed using a system of equations created by the direct differentiation of the equations used in DBEM. These will be evaluated by differentiation of the standard boundary conditions used in the deterministic system. Differentiating equations (4), (6) and (7) with respect to the design variable Z_m gives Mellings and Aliabadi (1993); Sfantos and Aliabadi (2006):

$$C_{ij,m}(\mathbf{x}')u_j(\mathbf{x}') + C_{ij}(\mathbf{x}')u_{j,m}(\mathbf{x}') + \sum_{\gamma=1}^{M}\sum_{n=1}^{3} u_{j,m}^n(\mathbf{x})\mathrm{P}_{ij}^{\gamma n} + \sum_{\gamma=1}^{M}\sum_{n=1}^{3} u_j^n(\mathbf{x})\mathrm{P}_{ij,m}^{\gamma n}$$
$$= \sum_{\gamma=1}^{M}\sum_{n=1}^{3} t_{j,m}^n(\mathbf{x})\mathrm{Q}_{ij}^{\gamma n} + \sum_{\gamma=1}^{M}\sum_{n=1}^{3} t_j^n(\mathbf{x})\mathrm{Q}_{ij,m}^{\gamma n} \tag{10}$$

$$\frac{1}{2}u_{i,m}(\mathbf{x}')+\frac{1}{2}u_{i,m}(\mathbf{x}'')+\sum_{\gamma=1}^{M}\sum_{n=1}^{3}u^n_{j,m}(\mathbf{x})\mathrm{P}^{\gamma n}_{ij}+\sum_{\gamma=1}^{M}\sum_{n=1}^{3}u^n_{j}(\mathbf{x})\mathrm{P}^{\gamma n}_{ij,m}$$
$$=\sum_{\gamma=1}^{M}\sum_{n=1}^{3}t^n_{j,m}(\mathbf{x})\mathrm{Q}^{\gamma n}_{ij}+\sum_{\gamma=1}^{M}\sum_{n=1}^{3}t^n_{j}(\mathbf{x})\mathrm{Q}^{\gamma n}_{ij,m} \tag{11}$$

$$\frac{1}{2}t_{i,m}(\mathbf{x}')+\frac{1}{2}t_{i,m}(\mathbf{x}'')+\sum_{\gamma=1}^{M}\sum_{n=1}^{3}u^n_{j,m}(\mathbf{x})\mathrm{V}^{\gamma n}_{kij}+\sum_{\gamma=1}^{M}\sum_{n=1}^{3}u^n_{j}(\mathbf{x})\mathrm{V}^{\gamma n}_{kij,m}$$
$$=\sum_{\gamma=1}^{M}\sum_{n=1}^{3}t^n_{j,m}(\mathbf{x})\mathrm{W}^{\gamma n}_{kij}+\sum_{\gamma=1}^{M}\sum_{n=1}^{3}t^n_{j}(\mathbf{x})\mathrm{W}^{\gamma n}_{kij,m} \tag{12}$$

where $()_{,m}$ indicates a derivative with respect to the design variable Z_m. The detail of the derivatives of coefficients $\mathrm{P}^{\gamma n}_{ij,m}$, $\mathrm{Q}^{\gamma n}_{ij,m}$, $\mathrm{V}^{\gamma n}_{kij,m}$, and $\mathrm{W}^{\gamma n}_{kij,m}$; the derivatives of fundamental solutions $T_{ij,m}$, $U_{ij,m}$, $D_{kij,m}$, $S_{kij,m}$ and the derivatives of Jacobian of transformation $J_{,m}$ can be found in (Appendix A:).

The equations (11) and (12) contain the required displacement and traction derivatives $u^n_{k,m}(\mathbf{x})$ and $t^n_{k,m}(\mathbf{x})$ which can now be used to analyse the derivatives of fracture parameters. In order to use the derivative of the system of equations to evaluate the response derivatives, it is necessary to prescribe a new set of boundary conditions for the derivative values. Since the known displacements and tractions at the boundary nodes are independent of the boundary geometry, their derivatives with respect to Z_m equal to 0.

After applying the new boundary condition, the derivative of the system of equations can be written in matrix form as:

$$\mathbf{A}\mathbf{X}_{,m}=\mathbf{F}_{,m}-\mathbf{A}_{,m}\mathbf{X} \tag{13}$$

where $\mathbf{X}_{,m}$ is the first order derivative of the unknown displacement and traction vector, $\mathbf{A}_{,m}$ is the first order derivative of the coefficient matrix, while $\mathbf{X}$ is the vector of known values at this stage. For the derivative analysis, the same coefficient matrix $\mathbf{A}$ that was used to solve the deterministic problem is reused here.

2.3 Analytic integration

The singular term in equation (4) is evaluated by the rigid body condition. Whereas the other singular and hyper-singular terms in equations (6) and (7) are calculated analytically. In the DBEM, since the crack is traction free, integrals involving U_{ij} and D_{kij} kernels are not required. The integrals required are those containing the T_{ij} terms in the displacement equation (6) and S_{kij} terms in the traction equation (7)

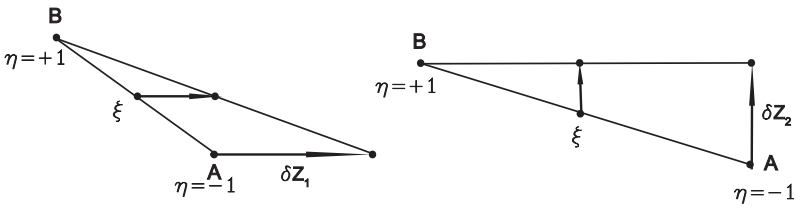

Figure 1: change to node A of a straight crack

when the field point is on the crack boundary. Further detail of the evaluation of the integrals contain T_{ij} and S_{kij} terms can be found in Portela, Aliabadi, and Rooke (1992, 1993).

In derivative DBEM analysis, the integrals requiring analytically calculation are those containing the $T_{ij,m}$ terms in equation (11) and $S_{kij,m}$ terms in equation (12). Since the crack faces are modelled as straight lines, therefore, the design variables are restricted to the coordinates of the end points of one or more crack elements in this work. Both the non-singular and the singular terms of equations (11) and (12) can be evaluated using the same approach adopted by Portela, Aliabadi, and Rooke (1992, 1993) on the basis of the geometric derivatives.

Consider a flat, boundary element with the end nodes labelled as A and B, as shown in Fig 1. The local coordinates of the end nodes are given by $\xi = \eta$. Assume the design variables related to the coordinates of these end nodes. Then a change in the design variable is a change in one direction of one of the end nodes, with the other end node remaining fixed. Applying a simple parametric function, the derivatives of the element node with respect to the design variable Z_m can be written in generalised form as:

$$x_{i,z_m} = \frac{(1+\eta\xi)}{2}\delta_{im} \tag{14}$$

$$\delta_{im} = \begin{cases} 1 & if \ Z_m \text{ represents a change in direction i} \\ 0 & \text{otherwise} \end{cases} \tag{15}$$

Using above definitions, the other required derivatives can be simplified. The integral which required analytical integration then reduces to:

$$u_j^n(\mathbf{x}) \int_{-1}^{+1} (T_{ij,m}(\mathbf{x}', \mathbf{x}(\xi)) J^\gamma(\xi) + T_{ij}(\mathbf{x}', \mathbf{x}(\xi)) J^\gamma_{,m}(\xi)) M^n(\xi) d\xi = 0 \tag{16}$$

$$u_j^n(\mathbf{x}) \int_{-1}^{+1} (S_{kij,m}(\mathbf{x}', \mathbf{x}(\xi)) J(\xi) + S_{kij}(\mathbf{x}', \mathbf{x}(\xi)) J_{,m}^{\gamma}(\xi)) M^n(\xi) d\xi$$

$$= \frac{E\eta}{2\pi l^2 (1-\nu^2)} h_{kij,m}^n u_j^n \int_{-1}^{+1} \frac{M^n(\xi)}{(\xi - \xi')^2} d\xi \tag{17}$$

where the terms $h_m^n = h_{kij,m}^n$ is given by

$$h_m^n = \begin{bmatrix} 2n_1n_2(4n_2^2-1) & -8n_2^2n_1^2+1 \\ 2n_1n_2(4n_1^2-1) & 8n_2^2n_1^2-4n_1^2+1 \\ -8n_2^2n_1^2+1 & 2n_1n_2(-4n_2^2+3) \end{bmatrix} \begin{matrix} for\ a\ change\ Z_m \\ in\ direction\ 1 \end{matrix} \tag{18}$$

$$h_m^n = \begin{bmatrix} -8n_2^2n_1^2+4n_2^2-1 & 2n_1n_2(-4n_2^2+1) \\ 8n_2^2n_1^2-1 & 2n_1n_2(-4n_1^2+1) \\ 2n_1n_2(4n_1^2-3) & 8n_2^2n_1^2-1 \end{bmatrix} \begin{matrix} for\ a\ change\ Z_m \\ in\ direction\ 2 \end{matrix} \tag{19}$$

3 The J-Integral and its derivatives

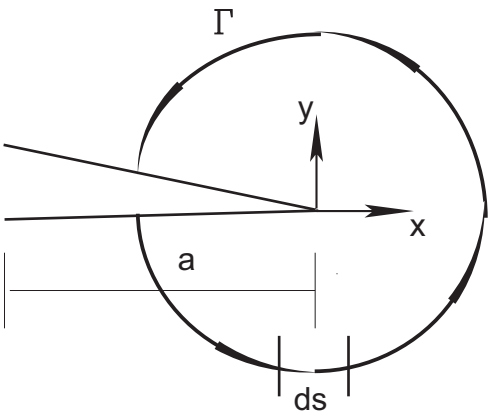

Figure 2: J-integral

One of the most popular path independent integrals is the J-integral, which can be defined as Rigby and Aliabadi (1993):

$$J = \int_{\Gamma} (W n_1 - t_j u_{j,1})\, d\Gamma \tag{20}$$

where W is the strain energy density, Γ is the contour, $d\Gamma$ is the differential length along contour Γ, $t_j = \sigma_{ij} n_j$ is the traction on the contour, n_j is the components of the unit vector normal to contour. Consider a body with a crack of length a, subjected to mode-I loading. Using an arbitrary counter-clockwise path around the crack tip, as shown in Figure 2, the relation between J and stress intensity factor is given by:

$$J = \frac{K_I^2 + K_{II}^2}{E'} \tag{21}$$

where $E' = E/(1-\nu^2)$ for plane strain condition. By using decomposition method, stress intensity factor for each mode can be obtained. The J-integral is an effective tool for the evaluation of the stress intensity factors, because the interior elastic field can be accurately determined along the contour path in the boundary element method, since the exact variation of the interior elastic field is built into the fundamental solution. Similar process can be applied to determine the derivatives of J and stress intensity factor. Differentiating the J with respect to design variable Z_m gives:

$$J_{,m} = \int_\Gamma \left[W_{,m} n_1 + W n_{1,m} - (t_{1,m}\varepsilon_{11} + t_1 \varepsilon_{11,m} + t_{2,m} \frac{\partial u_2}{\partial x_1} + t_2 \frac{\partial u_{2,m}}{\partial x_1}) \right] d\Gamma \tag{22}$$

The detail of those term in J and $J_{,m}$ are shown in Appendix B:.

4 Fatigue crack growth and its derivatives

4.1 Crack growth direction

Here, crack growth is simulated by an incremental crack extension, that assumes a piece-wise linear discretisation of crack path. For each increment analysis, crack extension is conveniently modelled with new boundary elements. In such a way, no remeshing is needed during crack extension. The local crack growth direction θ_t is determined by the condition that local shear stress is zero, that is:

$$K_I sin\theta_t + K_{II}(3cos\theta_t - 1) = 0 \tag{23}$$

where θ_t is the angular coordinate of the tangent to the crack path, centred at the crack tip and measured from the crack axis ahead of the crack tip.

In a mixed-mode analysis, an equivalent mode I stress intensity factor is defined as:

$$K_{I_{eq}} = K_I cos^3 \frac{\theta}{2} - 3K_{II} cos^2 \frac{\theta}{2} sin\frac{\theta}{2} \tag{24}$$

4.2 Fatigue crack growth

The analysis of fatigue crack life envisages the problem of showing the relation between the number of cycles of loading and the increments of cracks to obtain the final life of the damaged structure. In order to show the variation in the number of loading cycles as a function of crack length, in the present work the fatigue life N is determined from the empirical Paris model defined as:

$$N = \int_{a_0}^{a_f} \frac{da}{C(\triangle K_{eff})^m} \tag{25}$$

where a_0 is the initial crack length, a_f is the final crack length, C and m are the fatigue parameters and $\triangle K_{eff}$ is the range of the effective stress intensity factor. Although $\triangle K_{eff} = \triangle K_{I_{eq}}$ when the maximum principal stress criterion is used, the model of Tanaka Tanaka (1974) was applied in the present work to determine $\triangle K_{eff}$.

$$\triangle K_{eff} = \sqrt{\triangle K_I^2 + 2\triangle K_{II}^2} \tag{26}$$

5 Reliability analysis by FORM

The performance function for fatigue crack growth can be defined as:

$$g(\mathrm{Z}) = N - N_s \tag{27}$$

where N is the fatigue life (resistance) and N_s is the service life (load).

The probability of failure P_f is calculated assuming a generic N-dimensional vector Z of random variables. The first-order reliability method is based on linear approximation of the performance function $g(\mathrm{Z}) = 0$ to an ideal situation where Z is a vector of independent Gaussian variable with zero means and unit standard deviation.

The probability of failures is then defined by:

$$P_f = \Phi(-\beta) \tag{28}$$

where $\Phi(Z_m)$ is the cumulative probability distribution function of a standard Gaussian random variable, β is the reliability index. g(Z)>0 represents a safe state while g(Z)<0 represents a failute state. Therefore the the reliability index β can be usd as a measure of reliability which is the distance between the hyper plane g(Z) from the origin in the reduced space.

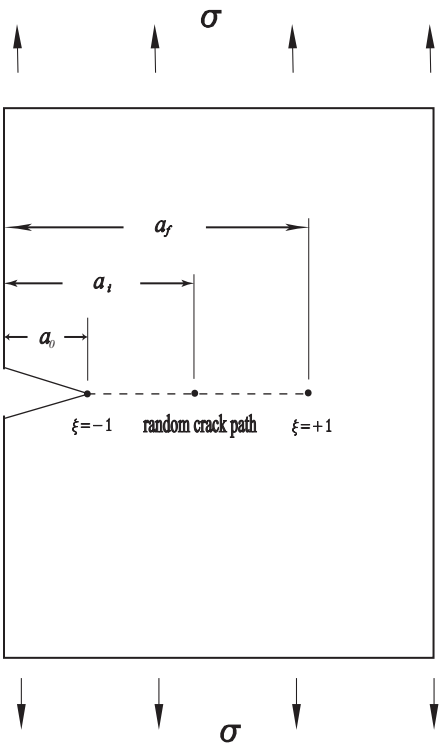

Figure 3: crack path

The Hasofer–Lind–Rackwitz–Fiessler algorithm Hasofer and Lind (1974); Rackwitz and Fiessler (1978) is used in this work to evaluate the failure point, which is applicable to nonlinear limit state functions. The number of iterations required for convergence to the design point depends on the degree of non-linearity of the limit state function in the transformation space.

5.1 Explicit expressions for derivatives of fatigue life

The random crack path is mapped to a local coordinate system, ξ, $\xi\ \varepsilon\ [-1,+1]$ (i.e., see Fig3) via a line mapping. For a straight or curved crack, the mapping from ξ to a (e.g., linear interpolation) is given by Besterfield, Liu, Lawrence, and Belytschko (1991):

$$a(\xi,Z) = \frac{1}{2}\left[(a_f - a_0)\xi + (a_f + a_0)\right] \tag{29}$$

Since the limits on the integration in (25) for the fatigue life are random, the crack path mapping is introduced in order to shift the randomness into the Jacobian.

Based on (25), the fatigue life is given by:

$$T = \int_{-1}^{+1} f\left[Z, K_{eq}(Z,\xi)\right] d\xi \tag{30}$$

where

$$f\left[Z, K_{eq}(Z,\xi)\right] = \frac{J(Z)}{C\left[K_{eq}(Z,\xi)\right]^m} \tag{31}$$

and the Jacobian of transformation, for the random variables Z, is defined by

$$J(Z) = \frac{1}{2}(a_f - a_0) \tag{32}$$

5.2 Total derivatives method

Total derivative method has been employed to calculate the response gradient. The total derivative of N with respect to the vector of random variables$Z$ can be written as:

$$\frac{dT}{dZ} = \int_{-1}^{+1} \left\{ f_{,Z} + f_{,K_{eq}} \left[K_{eq,K_I} \frac{\partial K_I(Z,\xi)}{\partial Z} + K_{eq,K_{II}} \frac{\partial K_{II}(Z,\xi)}{\partial Z} + K_{eq,\theta} \frac{\partial \theta(Z,\xi)}{\partial Z} \right] \right\} d\xi \tag{33}$$

where $f_{,Z}$, $f_{,K_{eq}}$, K_{eq,K_I}, $K_{eq,K_{II}}$ and $K_{eq,\theta}$ can be determined explicitly and are given in Appendix C.

Using the proposed method, $\frac{\partial K_I(Z,\xi)}{\partial Z}$ and $\frac{\partial K_{II}(Z,\xi)}{\partial Z}$ can be directly obtained using DBEM with IDM, while in this study does not account for the effect of the crack growth direction law that results in $\frac{\partial \theta(Z,\xi)}{\partial Z} = 0$ has not been accounted for. Further detail of the deviation relate to $\frac{\partial \theta(Z,\xi)}{\partial Z} = 0$ can be found in Appendix C:.

6 Numerical examples

6.1 Fatigue crack growth reliability analysis of double edge crack specimen

Consider a double edge crack specimen with the width $2W$ and the length $L = 3W$ as shown in Figure 4. The initial crack length a_0, final crack length a_f, fatigue parameters C, m and far-field tensile stress σ were treated as statistically independent random variables. Table 1 presents the mean, standard deviation and probability distribution for each of these random parameters. The Young's modulus E

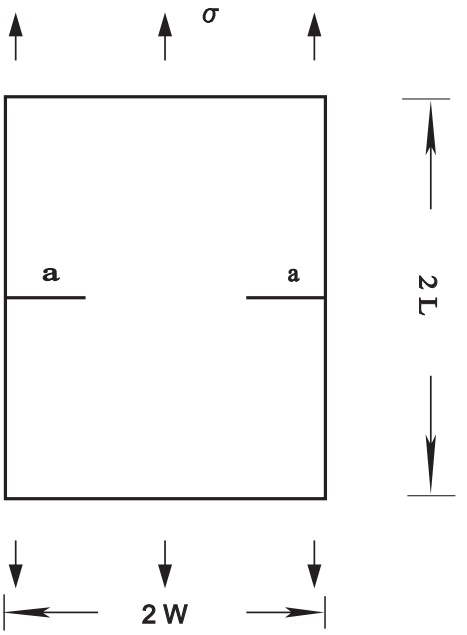

Figure 4: Geometry and loads of double edge crack specimen

Table 1: Statistical properties of random parameters

Parameters	Mean	Standard deviation	Probability distribution
Normalised initial crack length $\frac{a_0}{W}$	0.1	0.25	Normal
Normalised final crack length $\frac{a_f}{W}$	0.4	0.1	Normal
Fatigue parameter C	1.0×10^{-10}	3.0×10^{-11}	Normal
Fatigue parameter m	3.25	0.08	Normal
Normalised far-field tensile stress $\frac{\sigma}{E}$	4.0×10^{-4}	1.0×10^{-4}	Normal

and Poisson's ratio of $\upsilon = 0.3$ were assumed to be deterministic. The stress ratio $R = 0.1$ and the plane strain condition is assumed. Various values of the service life are assumed to be known and used in the probabilistic analysis.

The crack was assumed to be growing in 4 different increments with 5, 10, 15 and 20 propagation steps. For a known final crack size the normalised crack increment length $\frac{\triangle a}{W}$ are equal to 0.06, 0.03, 0.02 and 0.015, respectively. Half of the plate is

only modelled due to symmetry. Figure 5 shows the boundary conditions and the discretisation using 46 quadratic elements. The BEM model employed 30 continuous elements on the external boundary, while each crack face is discretised using 8 quadratic discontinuous elements. In the model with 96 quadratic elements, 18 quadratic discontinuous elements were used on each crack face, while the external boundary was modelled with 60 elements.

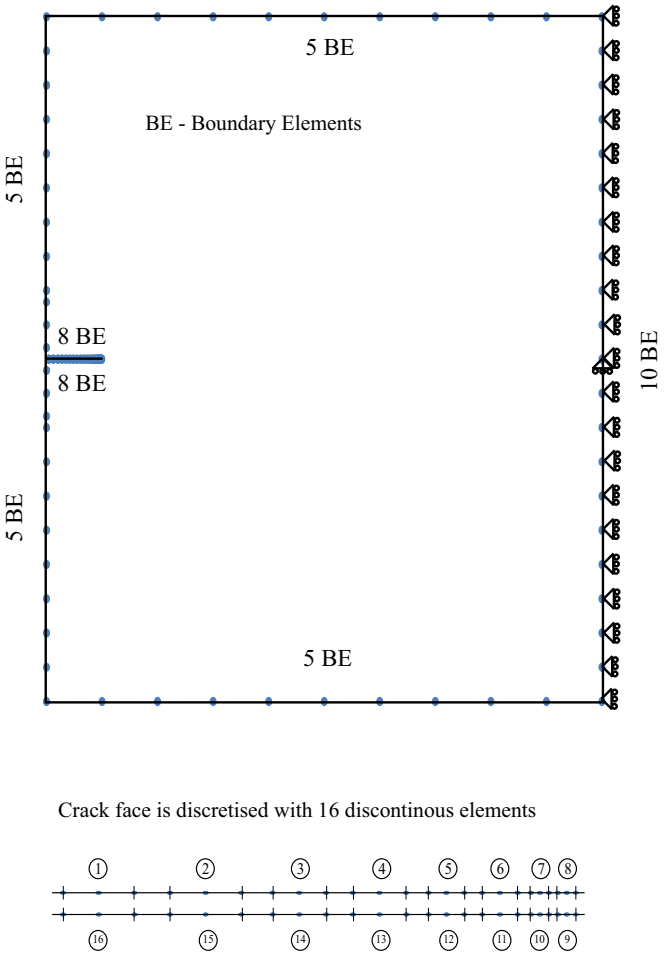

Figure 5: Boundary conditions and discretisation of double edge crack specimen

Figures 6 to 13 show the normalised values of stress intensity factors and its derivative with respect to the crack size for different crack growth sizes. Figures 6 to 9 show the stress intensity factors obtained by different boundary modelling. As it is

illustrated in the figures, the stress intensity factor increases with each crack growth and the maximum difference between the computational results from DBEM and analytical solutions provided by Tada, Paris, and Irwin (2000) is less than 0.14%. Figures 10 to 13 show the normalised value of derivatives of stress intensity factor with respect to crack size computed for different crack growth increment. As it can be seen in those figures, the results obtained by the DBEM agree well with the analytical solutions, with a maximum difference of 2.32%. The model with more boundary elements gives better evaluation of the derivatives of the stress intensity factor with respect to the crack size at each crack growth increment, although it does not improve the calculation of the stress intensity factor itself.

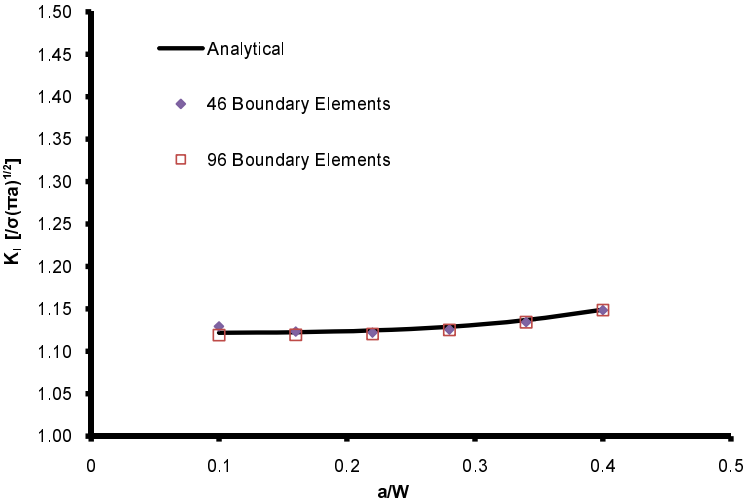

Figure 6: Normalised K_I with crack growth size $\frac{\triangle a}{W} = 0.06$

The increased difference in the derivative values is due to the new boundary elements introduced at each increment. In addition the analytical solution in Tada, Paris, and Irwin (2000) is based on an infinite plate which could also attribute to the difference in derivative analysis. A new assumption has to be made at each increment to define the new random variable, as the analytical integration has to be performed based on the new crack tip element illustrated in Figure 1. It is well recognized that any small difference between the calculation of the stress intensity factor by the reference solution and the BEM solution will give a larger error in the fatigue life; also the increased difference in the calculation of the derivatives of the stress intensity factor with respect to the crack size could induce an even larger difference in the reliability index.

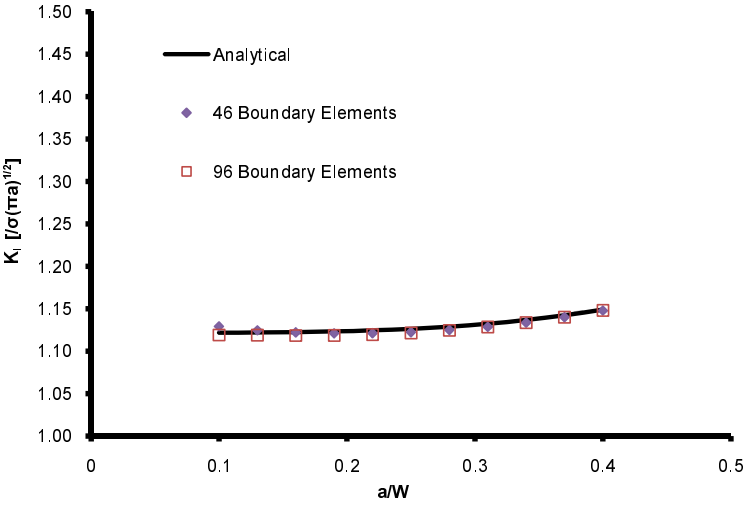

Figure 7: Normalised K_I with crack growth size $\frac{\triangle a}{W} = 0.03$

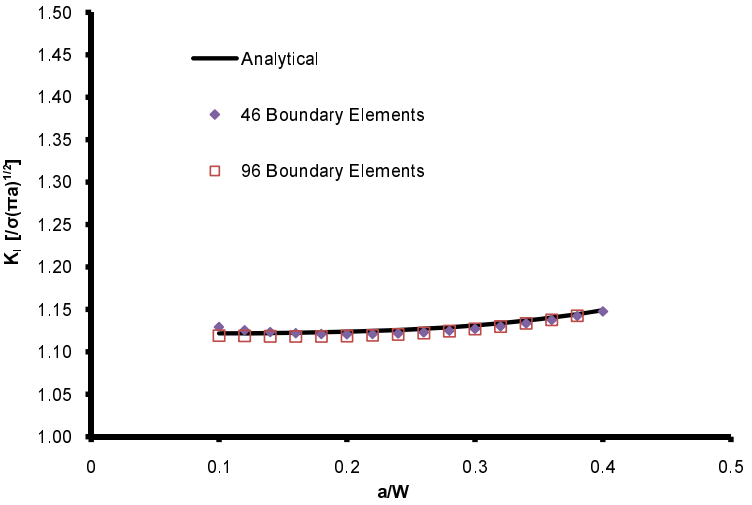

Figure 8: Normalised K_I with crack growth size $\frac{\triangle a}{W} = 0.02$

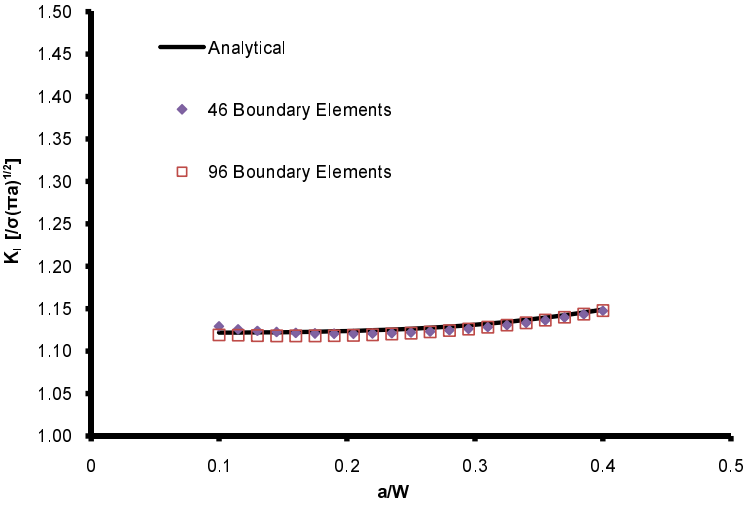

Figure 9: Normalised K_I with crack growth size $\frac{\triangle a}{W} = 0.015$

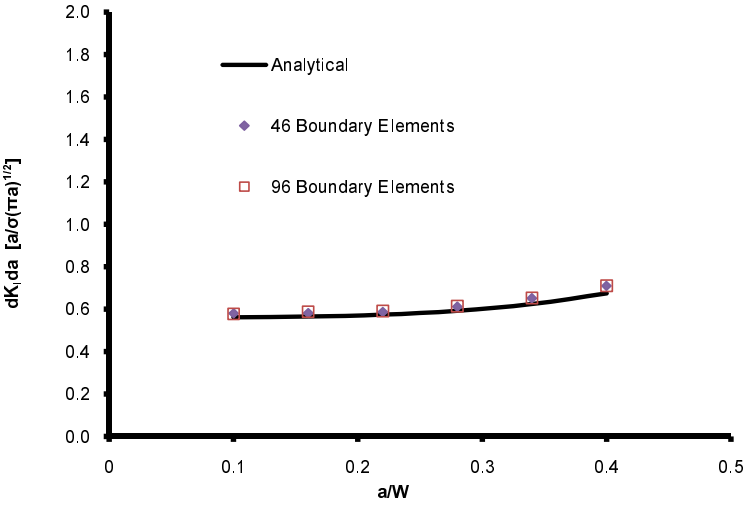

Figure 10: Normalised $\frac{\partial K_I}{\partial a}$ with crack growth size $\frac{\triangle a}{W} = 0.06$

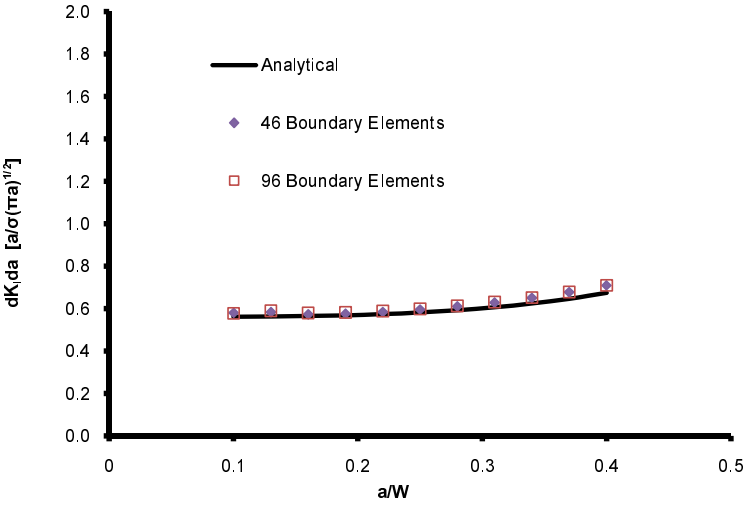

Figure 11: Normalised $\frac{\partial K_I}{\partial a}$ with crack growth size $\frac{\triangle a}{W} = 0.03$

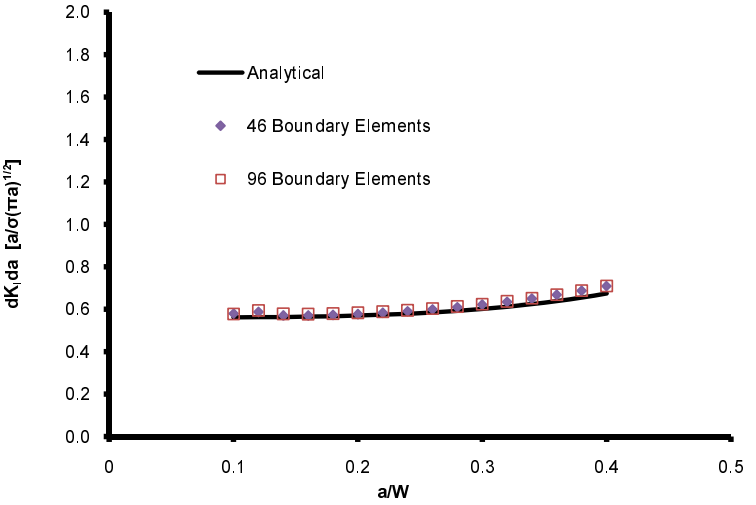

Figure 12: Normalised $\frac{\partial K_I}{\partial a}$ with crack growth size with IDM $\frac{\triangle a}{W} = 0.02$

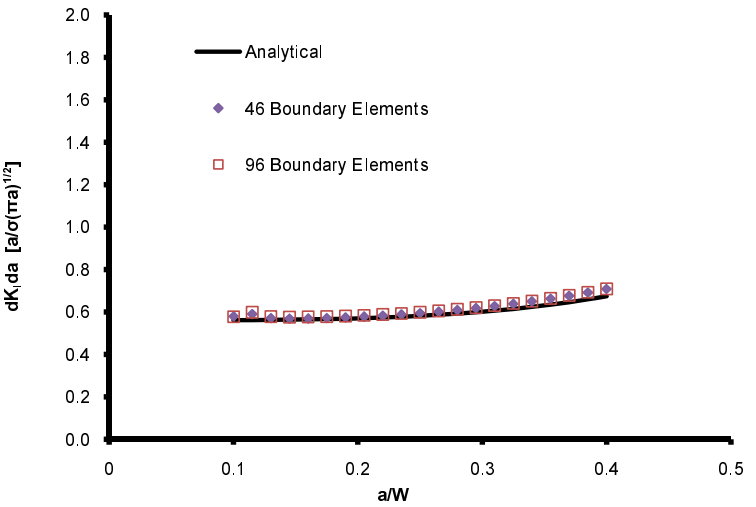

Figure 13: Normalised $\frac{\partial K_I}{\partial a}$ with crack growth size $\frac{\triangle a}{W} = 0.015$

The effect of the different crack increment size on the K_I and its derivatives was also investigated. Figures 14 to 17 show BEM solutions for the same number of the boundary elements used with different crack increment size compared to the analytical solution. The results in these Figures illustrate the normalised crack increment size $\frac{\triangle a}{W}$ equal to 0.06, 0.03, 0.02 and 0.015 which all have good evaluation of the stress intensity factor and its derivatives. Similarly as before, The model with more boundary elements improved the evaluation of the derivatives of the stress intensity factor with respect to the crack size at each crack growth increment, without any noticable improvement of the stress intensity factor.

The reliability index β is plotted as a function of the service life under various types of uncertainties in Figures 18 to 23. The model with 96 boundary elements is used, the crack is assumed to grow in 10 propagation steps. The Monte Carlo simulation with deterministic solution of the Paris law is used to validate the result obtained by the proposed method. Three different number of simulations are used to study the accuracy and efficiency of the Monte Carlo simulation. In this particular example, 1×10^5, 5×10^5 and one million simulations are used. As it can be seen in Figures 18 to 23, by increasing the number of simulations, the reliability index converges to the numerical value. The results demonstrated that in order to obtain higher reliability index, e.i. the probability of failure equals to 1×10^{-6} , it would require one million simulation which is computationally expensive.

Figure 18 shows the combined effect of all the considered random parameters. In contrast, Figures 19 to 23, the initial crack length a_0, final crack length a_f, fa-

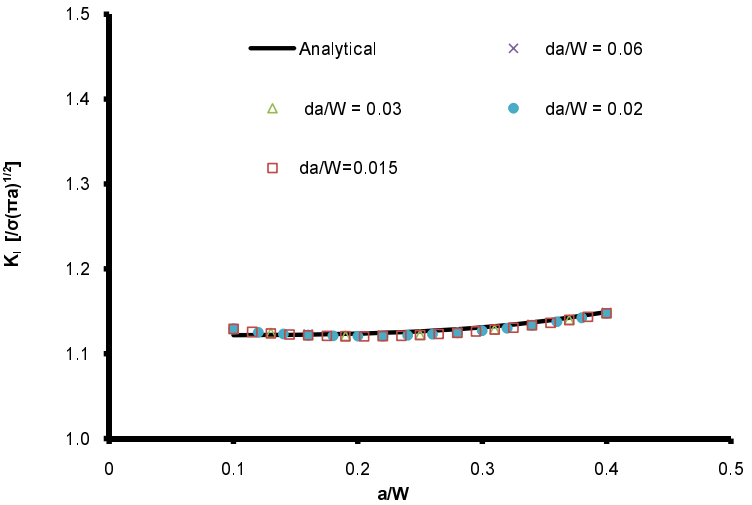

Figure 14: Normalised K_I with different crack increment sizes for total 46 boundary elements

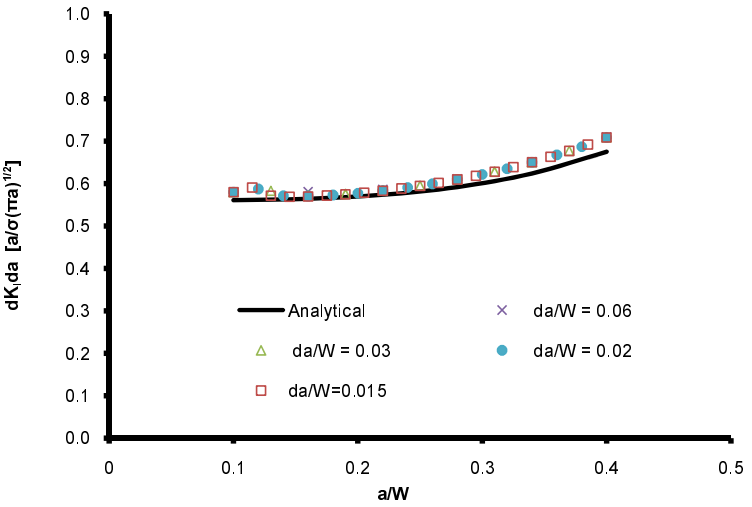

Figure 15: Normalised $\frac{\partial K_I}{\partial a}$ with different crack increment sizes for total 46 boundary elements

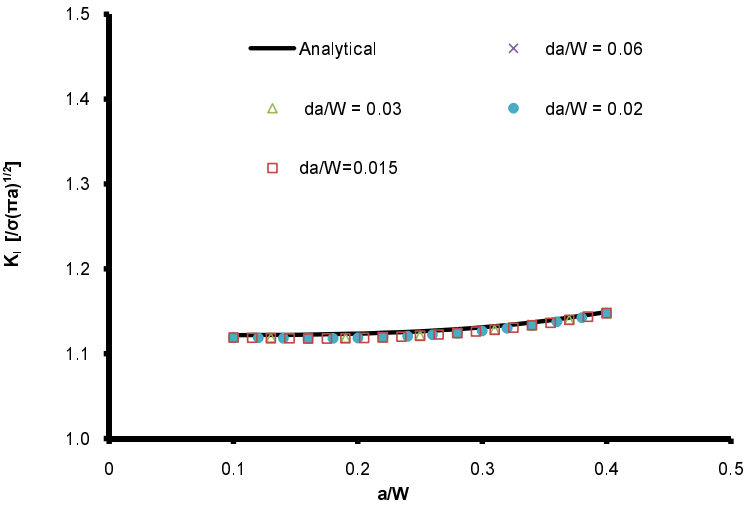

Figure 16: Normalised K_I with different crack increment sizes for total 96 boundary elements

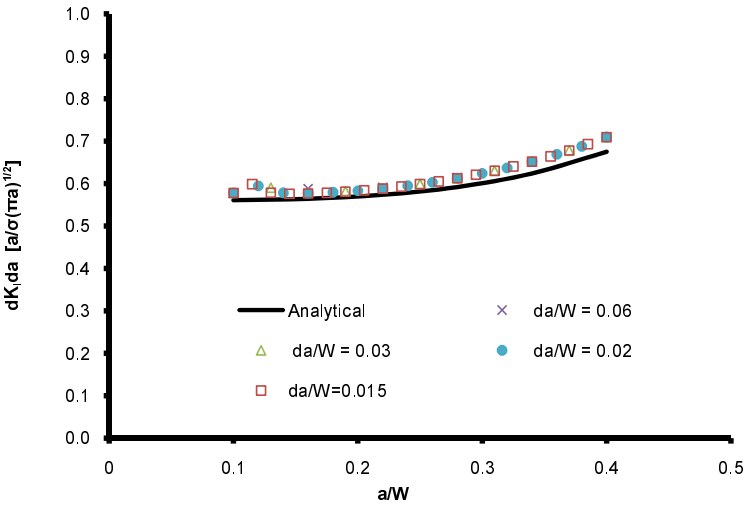

Figure 17: Normalised $\frac{\partial K_I}{\partial a}$ with different crack increment sizes for total 96 boundary elements

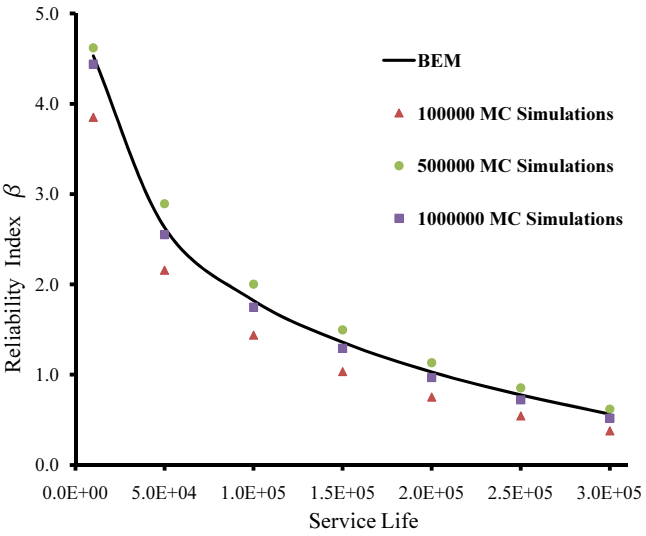

Figure 18: Reliability index with various uncertainty

tigue parameter C, fatigue parameter m and far-field tensile stress σ each has been modelled as a single random parameter separately, while the rest remained deterministic. As it can be seen from the graphs, all the numerical results obtained by BEM IDM agreed well with the results of the MC simulations (also obtained by running BEM). As expected, one million simulation yields the best result compared to 1×10^5 and 5×10^5 simulations. In Figure 24 all the numerical results for each random parameters are plotted in the same scale, which shows that the combination of all random parameters gives the smallest reliability index for a given service life which is expected. For a given reliability index (assuming $\beta = 4$), the final crack length a_f modelled as the only random variable yields the highest service life.

6.2 Fatigue crack growth reliability analysis of single edge crack specimen

Consider a single edge crack specimen with width W and length $L = 3W$ as shown in Figure 25. The initial crack length a_0, final crack length a_f, fatigue parameters C , m and far-field tensile stress σ were treated as statistically independent random variables. The mean, standard deviation and probability distribution for each of these random parameters are assumed to be the same as those given in Table 1. The Young's modulus E and Poisson's ratio of $\upsilon = 0.3$ were assumed to be deterministic. The stress ratio $R = 0.1$ and the plane stress condition is assumed.

A total of 96 boundary elements with 18 discontinuous elements on each of the crack face is used to model the specimen. The crack was assumed to be growing in

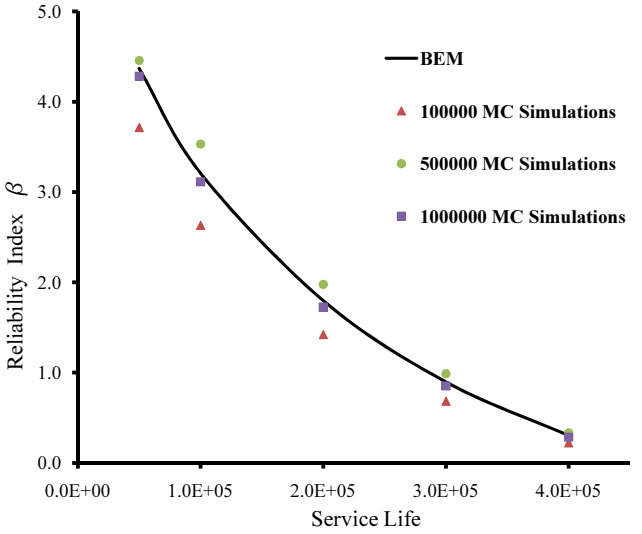

Figure 19: Reliability index with random initial crack length

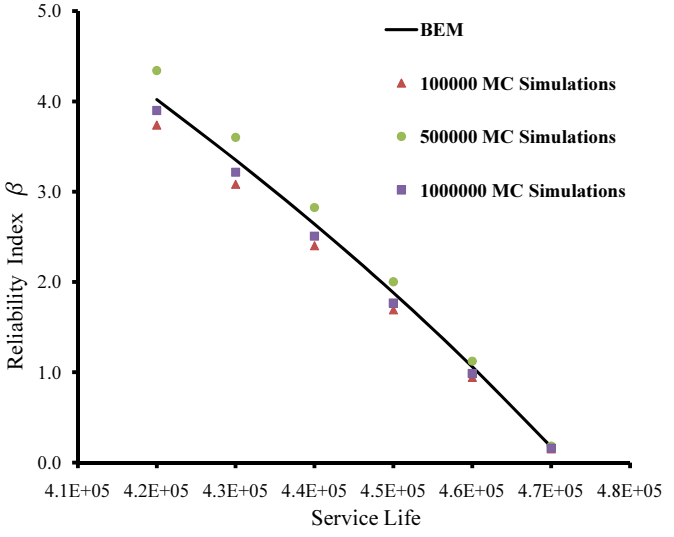

Figure 20: Reliability index with random final crack length

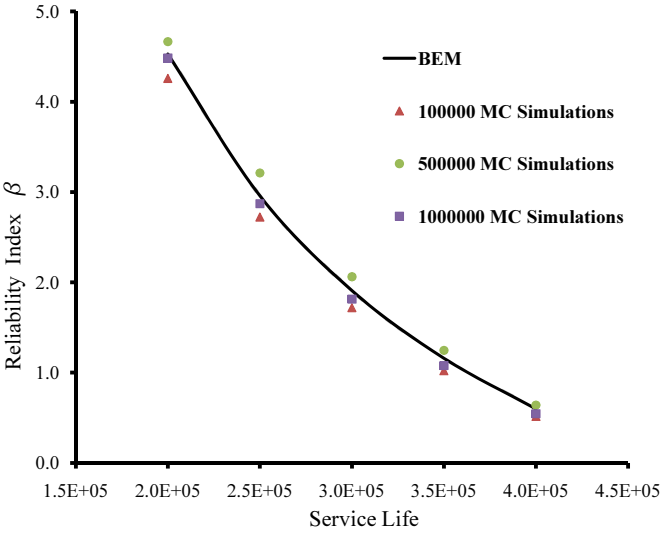

Figure 21: Reliability index with random fatigue parameter C

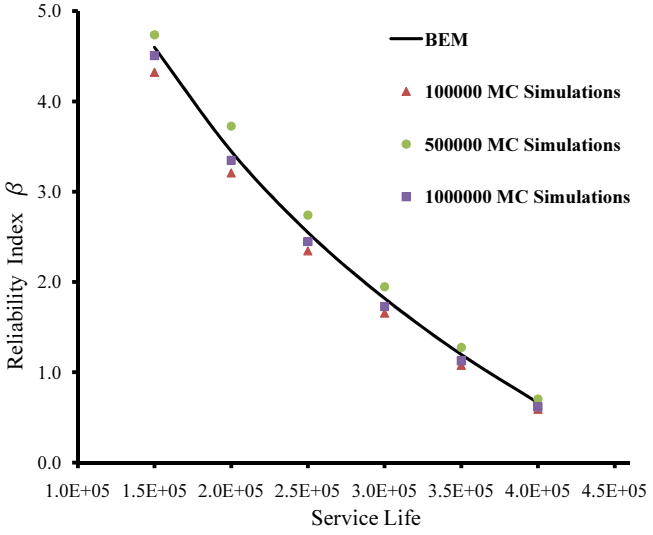

Figure 22: Reliability index with random fatigue parameter m

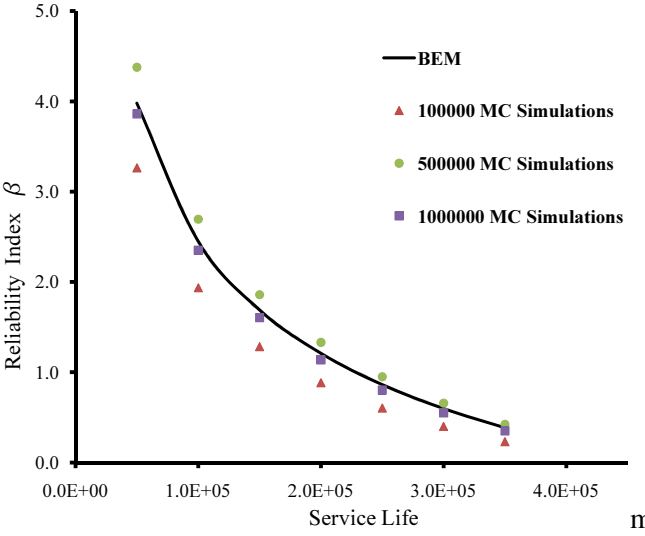

much

Figure 23: Reliability index with random stress

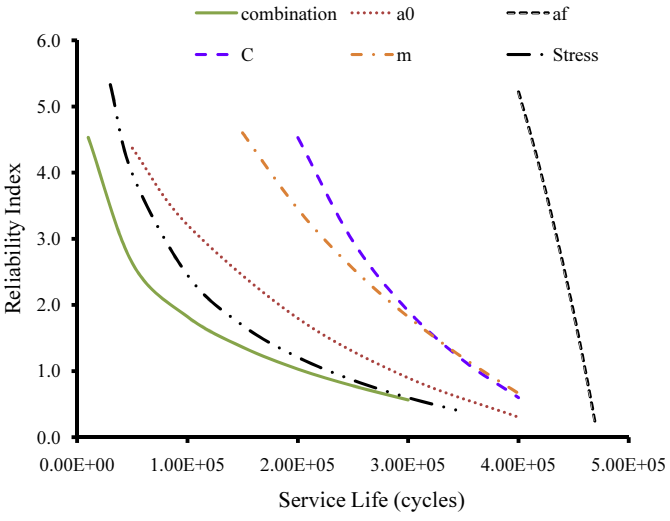

Figure 24: Comparison of random parameters

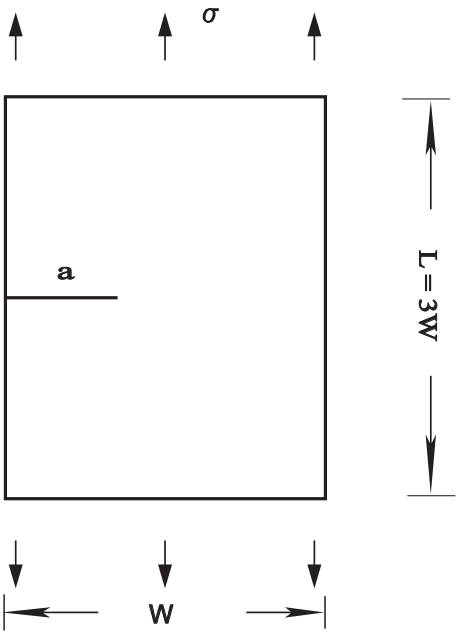

Figure 25: Geometry and loads of single edge crack specimen

4 different increments with 5, 10, 15 and 20 propagation steps. For a known final crack size the normalised crack increments $\frac{\triangle a}{W}$ are equal to 0.06, 0.03, 0.02 and 0.015, respectively.

Figure 26 shows the boundary conditions and the discretisation using 96 quadratic elements. The BEM model employed 60 continuous elements on the external boundary, while each crack face is discretised using 18 quadratic discontinuous elements. In the model with 46 quadratic elements, 8 quadratic discontinuous elements were used on each crack face, while the external boundary was modelled with 30 elements.

Figures 27 to 30 show the stress intensity factor and its derivatives with respect to cthe rack size at each crack growth increment. The stress intensity factor increases with each crack growth. The maximum difference between the BEM and the analytical solutions provided by Tada, Paris, and Irwin (2000) is less than 1%. The derivatives of the stress intensity factor with respect to the crack size at each crack growth are obtained by the BEM with IDM. As it can be seen in Figures 28 and 30, the results agree well with the analytical solution, with a maximum difference of 9%.

The reliability index is plotted as a function of the service life under the various

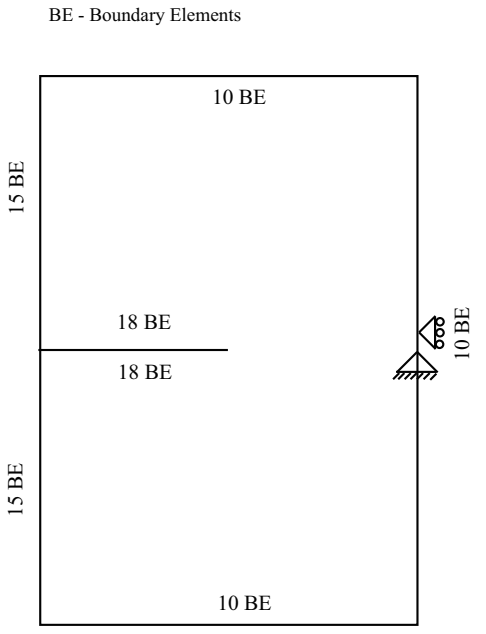

Figure 26: Boundary conditions and discretisation of single edge crack specimen

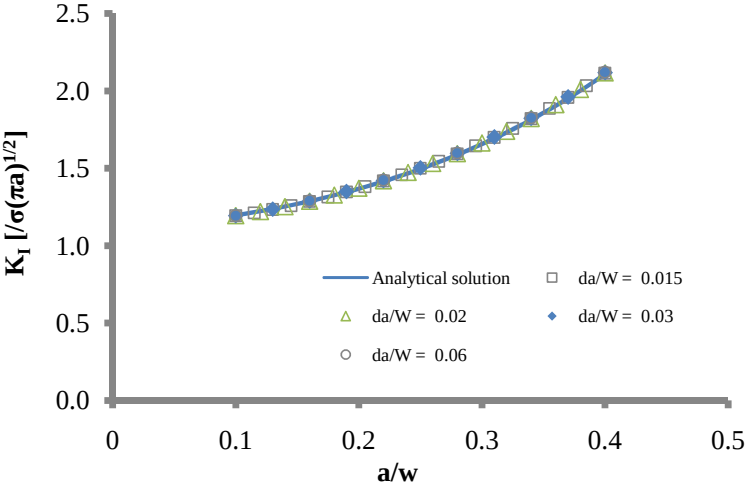

Figure 27: Normalised K_I with different crack increment sizes

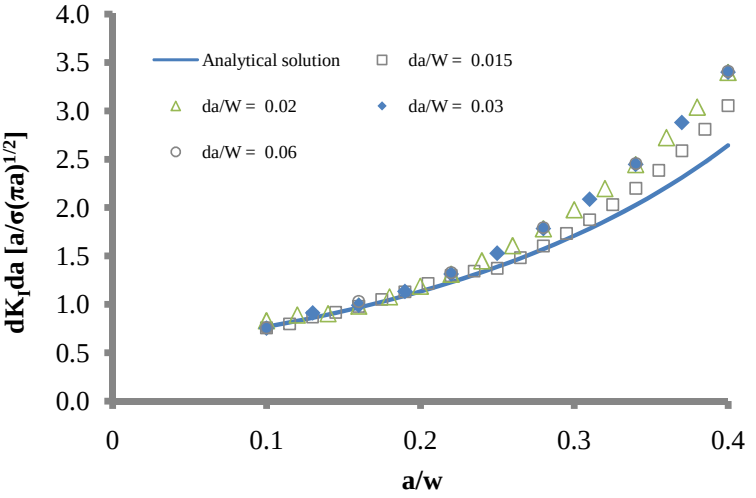

Figure 28: Normalised $\frac{\partial K_I}{\partial a}$ with different crack increment sizes

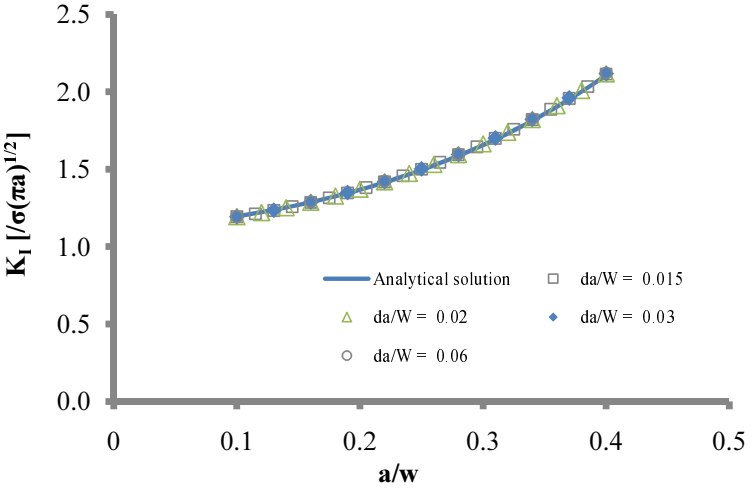

Figure 29: Normalised K_I with different crack increment sizes

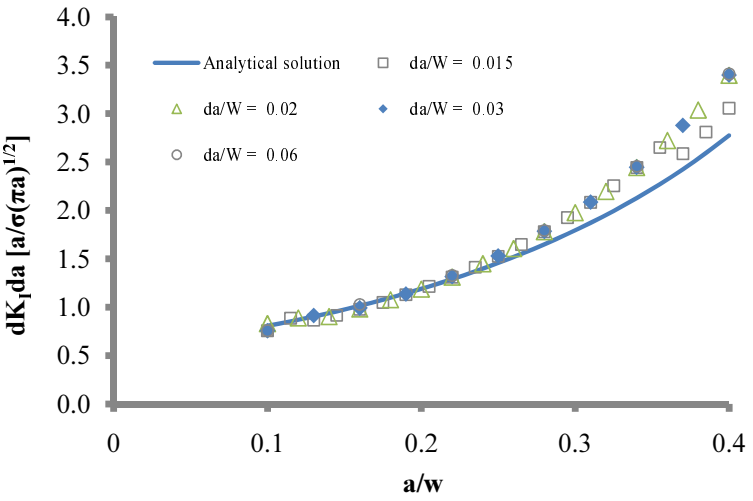

Figure 30: Normalised $\frac{\partial K_I}{\partial a}$ with different crack increment sizes

types of uncertainties in Figures 31 to 36. One million Monte Carlo simulations with deterministic solution of the Paris law was used in this example. In Figures 32 to 36 the initial crack length a_0, final crack length a_f, fatigue parameter C, fatigue parameter m, far-field tensile stress σ each has been modelled as a single random parameter, while Figure 31 shows the combined effect of all those random parameters. It can be seen that all of the numerical results agree well with the simulations.

It is essential to study the effect of different probability distribution functions on the reliability of the structure. Figure 37 shows the probability of failure P_f of the single edge crack specimen, as a function of service life. The initial crack length a_0 is treated as the only random variable with a mean value equal to 0.5 and standard deviation equal to 0.1 while different probability distribution functions are considered for the analysis. The probability of failure P_f obtained with Lognormal distribution has higher value compared to the one with Normal distribution in the tail region, while the Normal distribution yields higher probability of failure P_f around its mean value. Figure 37 also characterises the Cumulative Distribution Function (CDF) of the Normal and the Lognormal distributions for the probability of failure against the service life.

Throughout this work, the Normal and the Lognormal probability distributions have been used to characterize the random parameters. However, various probability distributions can be applied to evaluate the reliability in the illustrated examples.

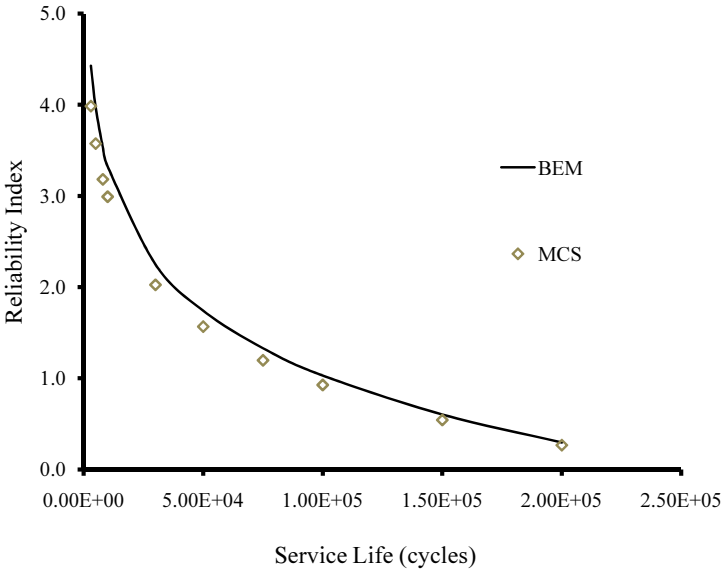

Figure 31: Reliability index with various uncertainty

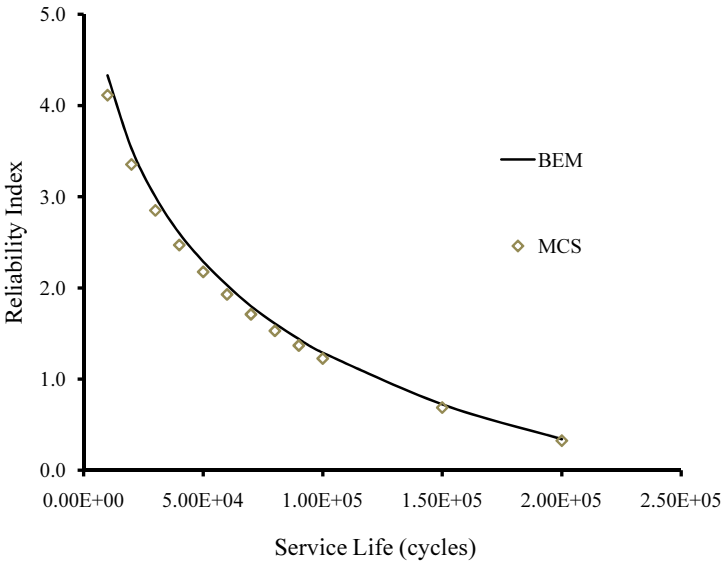

Figure 32: Reliability index with random initial crack length

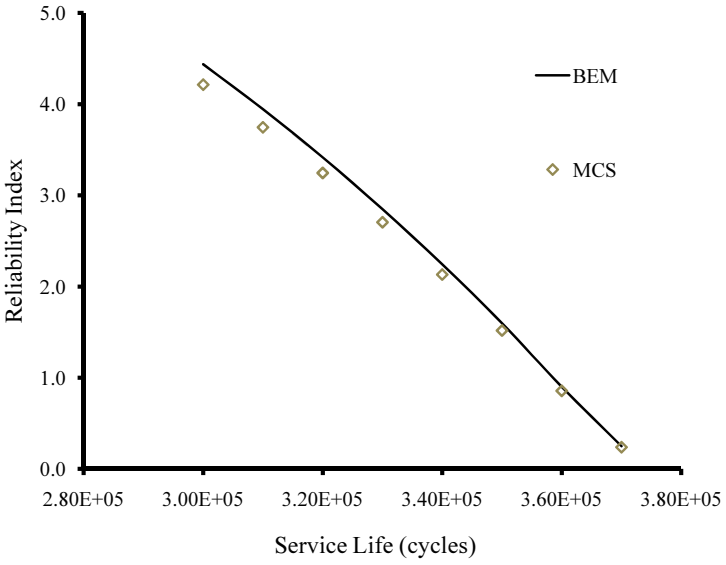

Figure 33: Reliability index with random final crack length

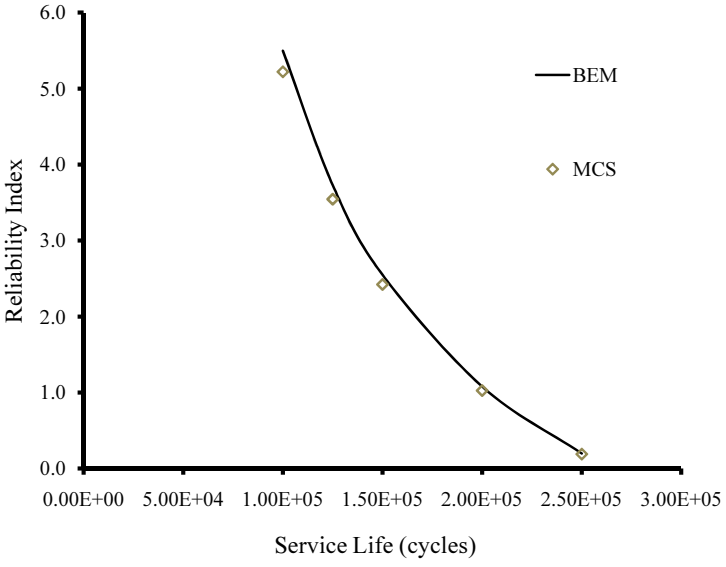

Figure 34: Reliability index with random fatigue parameter C

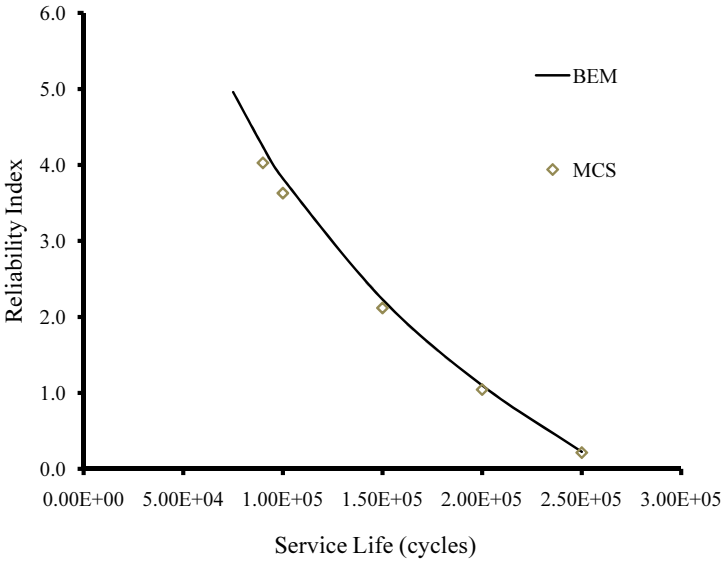

Figure 35: Reliability index with random fatigue parameter m

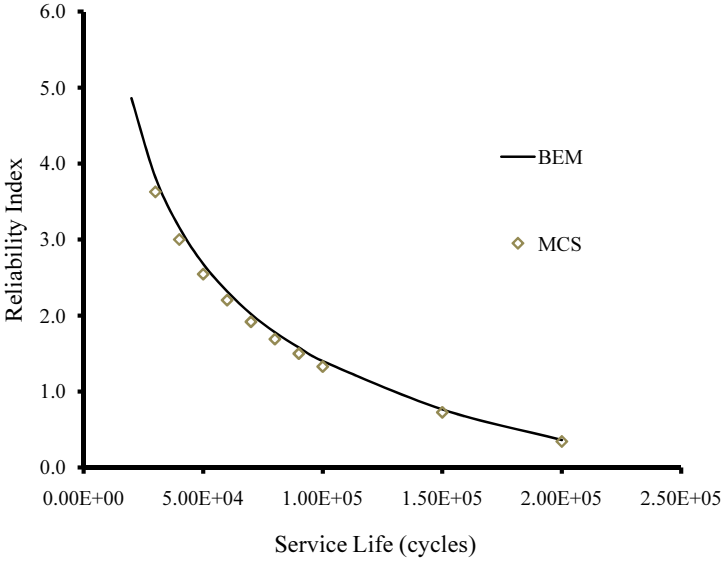

Figure 36: Reliability index with random stress

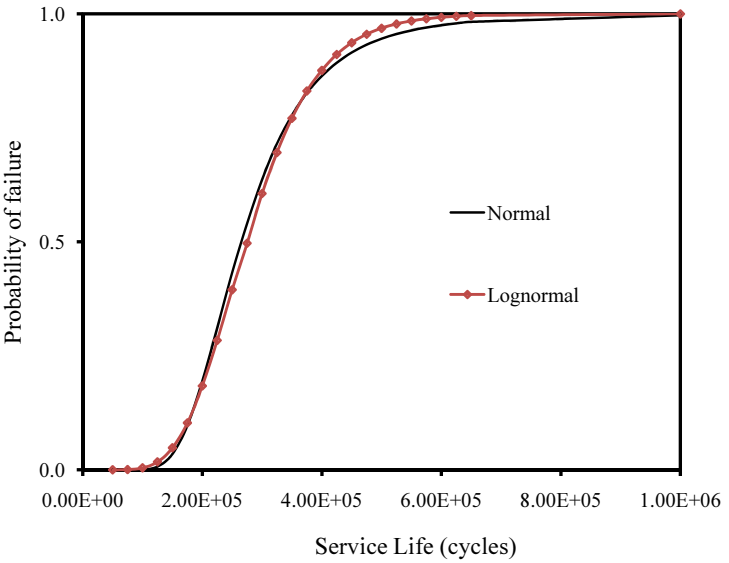

Figure 37: Comparison with different distribution

7 Conclusions

A method consisting of the DBEM coupled with FORM was developed to determine the reliability of fatigue crack growth. The method involves a total derivatives method for calculating the fatigue parameter derivatives with respect to random parameters. The Hasofer-Lind iterative technique is used to find the most probable point. The results obtained from the proposed method demonstrated good agreement with the Monte Carlo simulation, as DBEM provides very accurate calculation of the stress intensity factors and its derivatives leading to a good accuracy of the reliability index. Since all gradient are calculated analytically, the reliability analysis of fatigue crack growth can be performed efficiently using the proposed method.

References

Aliabadi, M. (2002): *The boundary element method, Volume II: Applications in Solids and Structures*. John Wiley & Sons Inc.

Benedetti, I.; Aliabadi, M.; Davi, G. (2008): A fast 3d dual boundary element method based on hierarchical matrices. *International journal of solids and structures*, vol. 45, no. 7, pp. 2355–2376.

Besterfield, G.; Liu, W.; Lawrence, M.; Belytschko, T. (1990): Brittle fracture reliability by probabilistic finite elements. *Journal of Engineering Mechanics*, vol. 116, no. 3, pp. 642–659.

Besterfield, G.; Liu, W.; Lawrence, M.; Belytschko, T. (1991): Fatigue crack growth reliability by probabilistic finite elements. *Computer methods in applied mechanics and engineering*, vol. 86, no. 3, pp. 297–320.

Chen, G.; Rahman, S.; Park, Y. (2001): Shape sensitivity and reliability analyses of linear-elastic cracked structures. *International Journal of Fracture*, vol. 112, no. 3, pp. 223–246.

Dirgantara, T.; Aliabadi, M. (2000): Crack growth analysis of plates loaded by bending and tension using dual boundary element method. *International journal of fracture*, vol. 105, no. 1, pp. 27–47.

Dong, L.; AtIuri, S. (2013): Fracture fatigue analyses: Sgbem-fem or xfem? part 2: 3d solids. *Computer Modeling in Engineering & Sciences*, vol. 90, no. 5, pp. 379 – 413.

Fedelinski, P.; Aliabadi, M.; Rooke, D. (1996): The laplace transform dbem for mixed-mode dynamic crack analysis. *Computers & structures*, vol. 59, no. 6, pp. 1021–1031.

Feng, G.; Garbatov, Y.; Guedes Soares, C. (2012): Probabilistic model of the growth of correlated cracks in a stiffened panel. *Engineering Fracture Mechanics*, vol. 84, pp. 83 – 95.

Graham-Brady, L.; Liu, J. (2013): Upscaling crack propagation and coalescence through a stochastic damage micromechanics model. pp. 191 – 193, New York, NY, United states.

Grigoriu, M.; Saif, M.; El Borgi, S.; Ingraffea, A. (1990): Mixed mode fracture initiation and trajectory prediction under random stresses. *International Journal of Fracture*, vol. 45, no. 1, pp. 19–34.

Guo, T.; Chen, Y.-W. (2013): Fatigue reliability analysis of steel bridge details based on field-monitored data and linear elastic fracture mechanics. *Structure and Infrastructure Engineering*, vol. 9, no. 5, pp. 496 – 505.

Harkness, H.; Belytschko, T.; Liu, W. (1992): Finite element reliability analysis of fatigue life. *Nuclear engineering and design*, vol. 133, no. 2, pp. 209–224.

Hasofer, A.; Lind, N. (1974): Exact and invariant second-moment code format. *Journal of the Engineering Mechanics Division*, vol. 100, no. 1, pp. 111–121.

Hombal, V.; Wolfe, K.; Ling, Y.; Mahadevan, S. (2012): Uncertainty quantification in non-planar crack growth analysis. pp. American Institute of Aeronautics and Astronautics (AIAA) –, Honolulu, HI, United states.

Katsuyama, J.; Itoh, H.; Li, Y.; Osakabe, K.; Onizawa, K.; Yoshimura, S. (2014): Benchmark analysis on probabilistic fracture mechanics analysis codes concerning fatigue crack growth in aged piping of nuclear power plants. *International Journal of Pressure Vessels and Piping*, vol. 117-118, pp. 56 – 63.

Leonel, E. D.; Chateauneuf, A.; Venturini, W. S. (2012): Probabilistic crack growth analyses using a boundary element model: Applications in linear elastic fracture and fatigue problems. *Engineering Analysis with Boundary Elements*, vol. 36, no. 6, pp. 944 – 959.

Li, H.; Xiang, Y.; Wang, L.; Zhang, J.; Liu, Y. (2013): Uncertainty propagation in fatigue crack growth analysis using dimension reduction technique. *International Journal of Reliability and Safety*, vol. 7, no. 3, pp. 293 – 317.

Lua, Y.; Liu, W.; Belytschko, T. (1993): Curvilinear fatigue crack reliability analysis by stochastic boundary element method. *International Journal for Numerical Methods in Engineering*, vol. 36, no. 22.

Mellings, S.; Aliabadi, M. (1993): Dual boundary element formulation for inverse potential problems in crack identification. *Engineering analysis with boundary elements*, vol. 12, no. 4, pp. 275–281.

Mi, Y.; Aliabadi, M. (1994): Three-dimensional crack growth simulation using BEM. *Computers & Structures*, vol. 52, no. 5, pp. 871–878.

Paffrath, M.; Wever, U. (2012): Stochastic integration methods: Comparison and application to reliability analysis. volume 7, pp. 383 – 396, Copenhagen, Denmark.

Peng, X.; Geng, L.; Liyan, W.; Liu, G.; Lam, K. (1998): A stochastic finite element method for fatigue reliability analysis of gear teeth subjected to bending. *Computational Mechanics*, vol. 21, no. 3, pp. 253–261.

Portela, A.; Aliabadi, M.; Rooke, D. (1992): The dual boundary element method: effective implementation for crack problems. *International Journal for Numerical Methods in Engineering*, vol. 33, no. 6.

Portela, A.; Aliabadi, M.; Rooke, D. (1993): Dual boundary element incremental analysis of crack propagation. *Computers and Structures*, vol. 46, no. 2, pp. 237–247.

Provan, J. (1987): Probabilistic fracture mechanics and reliability. *Martinus Nijhoff Publishers, P. O. Box 163, 3300 AD Dordrecht, The Netherlands, 1987. 467.*

Rackwitz, R.; Fiessler, B. (1978): Structural reliability under combined random load sequences. *Computers and structures*, vol. 9, no. 5, pp. 489–494.

Rebba, R.; Mahadevan, S. (2008): Computational methods for model reliability assessment. *Reliability Engineering & System Safety*, vol. 93, no. 8, pp. 1197–1207.

Rigby, R.; Aliabadi, M. (1993): Mixed-mode j-integral method for analysis of 3d fracture problems using bem. *Engineering Analysis with Boundary Elements*, vol. 11, no. 3, pp. 239–256.

Sankararaman, S.; Ling, Y.; Mahadevan, S. (2011): Uncertainty quantification and model validation of fatigue crack growth prediction. *Engineering Fracture Mechanics*, vol. 78, no. 7, pp. 1487–1504.

Sankararaman, S.; Ling, Y.; Shantz, C.; Mahadevan, S. (2011): Model calibration for fatigue crack growth analysis under uncertainty. In *Structural Dynamics, Volume 3*, pp. 387–394. Springer.

Schall, G.; Rackwitz, R.; Scharrer, M.; Ostergaard, C. (1991): Fatigue reliability investigation for marine structures using a response surface method. *Offshore Mechanics and Arctic Engineering–1991.*, vol. 2, pp. 247–254.

Sfantos, G.; Aliabadi, M. (2006): Wear simulation using an incremental sliding boundary element method. *Wear*, vol. 260, no. 9, pp. 1119–1128.

Sfantos, G.; Aliabadi, M. (2007): A boundary cohesive grain element formulation for modelling intergranular microfracture in polycrystalline brittle materials. *International journal for numerical methods in engineering*, vol. 69, no. 8, pp. 1590–1626.

Tada, H.; Paris, P.; Irwin, G. (2000): The stress analysis of cracks handbook. *American Society of Mechanical Engineers, 3 Park Avenue, New York, NY 10016-5990, USA, 2000.*, pp. 1–677.

Tanaka, K. (1974): Fatigue-Crack Propagation From a Crack Inclined to the Cyclic Tensile Axis. *Engineering Fracture Mechanics*, vol. 6, no. 3, pp. 493–507.

Wen, P.; Aliabadi, M.; Rooke, D. (1998): Cracks in three dimensions: A dynamic dual boundary element analysis. *Computer methods in applied mechanics and engineering*, vol. 167, no. 1, pp. 139–151.

Wen, P.; Aliabadi, M.; Rooke, D. (1998): Cracks in three dimensions: A dynamic dual boundary element analysis. *Computer methods in applied mechanics and engineering*, vol. 167, no. 1, pp. 139–151.

Zhu, W.; Lin, Y.; Lei, Y. (1992): On fatigue crack growth under random loading. *Engineering Fracture Mechanics*, vol. 43, no. 1, pp. 1–12.

Appendix A: Fundamental solutions and their derivatives

The detailed expressions for the first order derivatives of the coefficient terms $\mathrm{P}^{\gamma n}_{ij,m}$, $\mathrm{Q}^{\gamma n}_{ij,m}$, $\mathrm{V}^{\gamma n}_{kij,m}$ and $\mathrm{W}^{\gamma n}_{kij,m}$ with respect to the design variables Z_m, are given below:

$$\mathrm{P}^{\gamma n}_{ij,m} = \int_{-1}^{+1} T_{ij,m}(\mathbf{x}',\mathbf{x}(\xi))M^n(\xi)J^\gamma(\xi)d\xi + \int_{-1}^{+1} T_{ij}(\mathbf{x}',\mathbf{x}(\xi))M^n(\xi)J^\gamma_{,m}(\xi)d\xi \tag{34}$$

$$\mathrm{Q}^{\gamma n}_{ij,m} = \int_{-1}^{+1} U_{ij,m}(\mathbf{x}',\mathbf{x}(\xi))M^n(\xi)J^\gamma(\xi)d\xi + \int_{-1}^{+1} U_{ij}(\mathbf{x}',\mathbf{x}(\xi))M^n(\xi)J^\gamma_{,m}(\xi)d\xi \tag{35}$$

$$\mathrm{V}^{\gamma n}_{ij,m} = \int_{-1}^{+1} S_{kij,m}(\mathbf{x}',\mathbf{x}(\xi))M^n(\xi)J^\gamma(\xi)d\xi + \int_{-1}^{+1} S_{kij}(\mathbf{x}',\mathbf{x}(\xi))M^n(\xi)J^\gamma_{,m}(\xi)d\xi \tag{36}$$

$$\mathrm{Q}^{\gamma n}_{ij,m} = \int_{-1}^{+1} D_{kij,m}(\mathbf{x}',\mathbf{x}(\xi))M^n(\xi)J^\gamma(\xi)d\xi + \int_{-1}^{+1} D_{kij}(\mathbf{x}',\mathbf{x}(\xi))M^n(\xi)J^\gamma_{,m}(\xi)d\xi \tag{37}$$

The detailed expressions for the first order derivatives of the boundary element kernels with respect to the design variables Z_m, are given below:

$$U_{ij}(\mathbf{x}',\mathbf{x}) = \frac{1}{8\pi\mu(1-\nu)}\left\{r_{,i}r_{,j} - (3-4\nu)ln\left(\frac{1}{r}\right)\delta_{ij}\right\} \tag{38}$$

$$U_{ij,m}(\mathbf{x}',\mathbf{x}) = \frac{1}{8\pi\mu(1-\nu)r}\left\{r_{i,m}r_{,j} + r_{j,m}r_{,i} - [(3-4\nu)\delta_{ij} + 2r_{,i}r_{,j}]r_{,m}\right\} \tag{39}$$

$$T_{ij}(\mathbf{x}',\mathbf{x}) = \frac{-1}{4\pi(1-\nu)r}\left\{\frac{\partial r}{\partial n}[(1-2\nu)\delta_{ij} + 2r_{,i}r_{,j}] - (1-2\nu)(n_j r_{,i} - n_i r_{,j})\right\} \tag{40}$$

$$\begin{aligned} T_{ij,m}(\mathbf{x}',\mathbf{x}) = \frac{-1}{4\pi(1-\nu)r^2}\Big\{ & 2\frac{\partial r}{\partial n}[r_{i,m}r_{,j} + r_{j,m}r_{,i} - ((1-2\nu)\delta_{ij} + 4r_{,i}r_{,j})r_{,m}] \\ & + (r_k n_k)_{,m}[(1-2\nu)\delta_{ij} + 2r_{,i}r_{,j}] + (1-2\nu)(n_i r_{j,m} + n_{i,m}r_j \\ & - n_j r_{i,m} - n_{j,m}r_i) + 2(1-2\nu)(n_j r_{,i} - n_i r_{,j})r_{,m}\Big\} \end{aligned} \tag{41}$$

$$D_{kij}(\mathbf{x}',\mathbf{x}) = \frac{1}{4\pi(1-\nu)r}\left\{(1-2\nu)(\delta_{ik}r_{,j} + \delta_{jk}r_{,i} - \delta_{ij}r_{,k}) + 2r_{,i}r_{,j}r_{,k}\right\} \tag{42}$$

$$D_{kij,m}(\mathbf{x}',\mathbf{x}) = \frac{1}{4\pi(1-\nu)r^2}\left\{ \left[2r_{,i}r_{,k} + (1-2\nu)\delta_{ik}\right] r_{j,m} \right.$$
$$+ \left[2r_{,j}r_{,k} + (1-2\nu)\delta_{jk}\right] r_{i,m} + \left[2r_{,i}r_{,j} - (1-2\nu)\delta_{ij}\right] r_{k,m}$$
$$\left. 2\left[(1-2\nu)(\delta_{ik}r_{,j} + \delta_{jk}r_{,i} - \delta_{ij}r_{,k}) + 4r_{,i}r_{,j}r_{,k}\right] r_{,m} \right\}$$

$$S_{kij}(\mathbf{x}',\mathbf{x}) = \frac{E}{4\pi(1-\nu^2)r^2}\left\{ 2\frac{\partial r}{\partial n}\left[(1-2\nu)\,\delta_{ij}r_{,k} + \nu\left(\delta_{ik}r_{,j} + \delta_{jk}r_{,i}\right) - 4r_{,i}r_{,j}r_{,k}\right] \right.$$
$$+ \left[2\nu r_{,j}r_{,k} + (1-2\nu)\,\delta_{jk}\right] n_i + \left[2\nu r_{,i}r_{,k} + (1-2\nu)\,\delta_{ik}\right] n_j$$
$$\left. + \left[2\,(1-2\nu)\,r_{,i}r_{,j} - (1-4\nu)\,\delta_{ij}\right] n_k \right\} \tag{43}$$

$$S_{kij,m}(\mathbf{x}',\mathbf{x}) = \frac{E}{4\pi(1-\nu^2)r^3}\left\{ \left[2\nu r_{,j}r_{,k} + (1-2\nu)\delta_{jk}\right] n_{i,m}r \right.$$
$$+ \left[2\nu r_{,i}r_{,k} + (1-2\nu)\delta_{ik}\right] n_{j,m}r$$
$$+ \left[2(1-2\nu)r_{,i}r_{,j} - (1-4\nu)\delta_{ij}\right] n_{k,m}r$$
$$- 2\left[(4\nu r_{,j}r_{,k} + (1-2\nu)\delta_{jk})r_{,m} - \nu(r_{j,m}r_{,k} + r_{k,m}r_{,j})\right] n_i$$
$$- 2\left[(4\nu r_{,i}r_{,k} + (1-2\nu)\delta_{ik})r_{,m} - \nu(r_{i,m}r_{,k} + r_{k,m}r_{,i})\right] n_j$$
$$- 2\left[(4(1-2\nu)r_{,i}r_{,j} - (1-4\nu)\delta_{ij})r_{,m}\right. \tag{44}$$
$$\left. \left. -(1-2\nu)(r_{j,m}r_{,i} + r_{i,m}r_{,j})n_k\right] \right\}$$

The derivatives of the radius r given as:

$$r_{,m} = r_{,i}r_{i,m} \tag{45}$$

where

$$r_{,i} = \frac{r_i}{r} = \frac{x_i - x_i'}{r} = \frac{\partial r}{\partial x_i(\mathbf{x})} \tag{46}$$

$$r_{i,m} = \frac{\partial r_i}{\partial z_m} = x_{i,m}(\mathbf{x}) - x_{i,m}(\mathbf{x}') \tag{47}$$

and

$$\frac{\partial r}{\partial \mathrm{n}(\mathbf{x})} = \frac{\partial r}{\partial x_i(\mathbf{x})}\mathrm{n}_i = r_i\mathrm{n}_i \tag{48}$$

The field point coordinates are obtained using the interpolation function as:

$$x_i = \sum_{n=1}^{3} M^n(\xi) x_i^n \tag{49}$$

where x_i^n are the global nodal positions and $M^n(\xi)$ are the two dimensional quadratic shape functions.

The first order derivatives of the coordinates of the field point with respect to the design variables are given as:

$$x_{i,m} = \sum_{n=1}^{3} M^n(\xi) x_{i,m}^n \tag{50}$$

The Jacobian of transformation is given by:

$$J^\gamma(\xi) = \sqrt{\left(\frac{dx_1(\xi)}{d\xi}\right)^2 + \left(\frac{dx_2(\xi)}{d\xi}\right)^2} \tag{51}$$

$$\frac{dx_i(\xi)}{d\xi} = \sum_{n=1}^{3} \frac{dM^n(\xi)}{d\xi} x_i^n \tag{52}$$

And its derivative

$$J_{,m}^\gamma(\xi) = \frac{1}{J^\gamma(\xi)} \left\{ \frac{dx_1(\xi)}{d\xi} \left[\frac{dx_1(\xi)}{d\xi}\right]_{,m} + \frac{dx_2(\xi)}{d\xi} \left[\frac{dx_2(\xi)}{d\xi}\right]_{,m} \right\} \tag{53}$$

The components of the unit outward normal vector and their derivatives are:

$$n_1(\xi) = \frac{1}{J^\gamma(\xi)} \frac{dx_2(\xi)}{d\xi} \tag{54}$$

$$n_2(\xi) = -\frac{1}{J^\gamma(\xi)} \frac{dx_1(\xi)}{d\xi} \tag{55}$$

$$n_{1,m} = \frac{1}{J^\gamma(\xi)} \left[\left(\frac{dx_2(\xi)}{d\xi}\right)_{,m} - n_1(\xi) J_{,m}^\gamma(\xi) \right] \tag{56}$$

$$n_{2,m} = -\frac{1}{J^\gamma(\xi)} \left[\left(\frac{dx_1(\xi)}{d\xi}\right)_{,m} + n_2(\xi) J_{,m}^\gamma(\xi) \right] \tag{57}$$

Appendix B: J-integral and its derivatives

$$t_1 = \sigma_{11} n_1 + \sigma_{12} n_2 \tag{58}$$

$$t_2 = \sigma_{12} n_1 + \sigma_{22} n_2 \tag{59}$$

$$\varepsilon_{11} = \frac{1 - \nu^2}{E} \left(\sigma_{11} - \frac{\upsilon}{1 - \upsilon^2} \sigma_{22} \right) \tag{60}$$

$$\varepsilon_{22} = \frac{1-\nu^2}{E}\left(\sigma_{22} - \frac{\upsilon}{1-\upsilon^2}\sigma_{11}\right) \tag{61}$$

$$\varepsilon_{12} = \frac{2(1+\nu)}{E}\sigma_{12} \tag{62}$$

$$W = \frac{1}{2}(\sigma_{11}\varepsilon_{11} + \sigma_{22}\varepsilon_{22} + \sigma_{12}\varepsilon_{12}) \tag{63}$$

$$t_{1,m} = \sigma_{11,m}n_1 + \sigma_{11}n_{1,m} + \sigma_{12,m}n_2 + +\sigma_{12}n_{2,m} \tag{64}$$

$$t_{2,m} = \sigma_{12,m}n_1 + \sigma_{12}n_{1,m} + \sigma_{22,m}n_2 + \sigma_{22}n_{2,m} \tag{65}$$

$$\varepsilon_{11,m} = \frac{1-\nu^2}{E}\left(\sigma_{11,m} - \frac{\upsilon}{1-\upsilon^2}\sigma_{22,m}\right) \tag{66}$$

$$\varepsilon_{22,m} = \frac{1-\nu^2}{E}\left(\sigma_{22,m} - \frac{\upsilon}{1-\upsilon^2}\sigma_{11,m}\right) \tag{67}$$

$$\varepsilon_{12,m} = \frac{2(1+\nu)}{E}\sigma_{12,m} \tag{68}$$

$$W_{,m} = \frac{1}{2}\left(\sigma_{11,m}\varepsilon_{11} + \sigma_{11}\varepsilon_{11,m} + \sigma_{22,m}\varepsilon_{22} + \sigma_{22}\varepsilon_{22,m} + \sigma_{12,m}\varepsilon_{12} + \sigma_{12}\varepsilon_{12,m}\right) \tag{69}$$

Appendix C: Total derivatives of N

$$f_{,Z} = \frac{1}{C(K_{eq})^m}\left(\frac{\partial J}{\partial Z}\right) - \frac{1}{C^2(K_{eq})^m}\left(\frac{\partial C}{\partial Z}\right) - \frac{J\ln(K_{eq})}{C(K_{eq})^m}\left(\frac{\partial m}{\partial Z}\right) \tag{70}$$

$$f_{,K_i} = -\frac{mJ}{C(K_{eq})^{m+1}}\left(\frac{\partial K_{eq}}{\partial K_i}\right) \tag{71}$$

$$f_{,\theta_i} = -\frac{mJ}{C(K_{eq})^{m+1}}\left(\frac{\partial K_{eq}}{\partial \theta_i}\right) \tag{72}$$

$$K_{eq_{,K_i}} = \begin{bmatrix} cos^3\left(\frac{\theta_i}{2}\right) \\ -3cos^2\left(\frac{\theta_i}{2}\right)sin\left(\frac{\theta_i}{2}\right) \end{bmatrix} \tag{73}$$

$$K_{eq_{,K_i}} = 0 \tag{74}$$